Available online at www.sciencedirect.com
SCIENCE DIRECT®
International Journal of Heat and Mass Transfer 48 (2005) 2209–2218
International Journal of HEAT and MASS TRANSFER
www.elsevier.com/locate/ijhmt

# Momentum and mass transfer on sandpaper-roughened surfaces in pipe flow

Saimir A. Lolja *

*Department of Chemical Engineering, University of Toronto, 200 College Street, Toronto, ON, Canada, M5S 3E5*

Received 15 April 2004; received in revised form 31 December 2004
Available online 26 February 2005

**Abstract**

A series of three electrochemically obtained nickel pipes with different surface roughness degree has been used in this study. In respect to momentum transfer, these rough surfaces exhibit similar patterns in terms of friction factor, friction similarity function, and rough-to-smooth friction factor ratio. The mass transfer is investigated with the electrochemical technique which exploits the red-ox reactions of potassium ferri- and ferro-cyanides. The gain in mass transfer enhancement is positive against the friction development in the range 3000–30,000 for the Reynolds number.


*Keywords:* Momentum transfer; Mass transfer; Rough surface

## 1. Introduction

The nature of transport phenomena on rough surfaces is complex, because the Eddy diffusivity behaviour in close vicinity of the wall is not known with sufficient accuracy, and in particular for fluids with high Schmidt number. A given surface can be classified as "hydraulically smooth" when its roughness elements lie entirely within the viscous sub-layer. At high Schmidt numbers, where the resistance to mass transfer is mainly within the viscous sub-layer, the same surface can show a significant increase in transfer rates over those of a truly smooth surface. At high Reynolds number, the friction factor becomes constant, while heat and mass transfer coefficients continue to depend on fluid properties. The increasing Reynolds number is associated with the disruption of the viscous sub-layer and penetration of turbulence into the valley or hole regions, and thus it is associated with increased rates of both momentum and mass transfer. Regularly roughened surfaces (e.g. repeated grooves or ribs) are geometrically similar surfaces, and the ratio of pitch to height of a roughness element is truly a characterising parameter. On the other side, though the characterization of randomly rough surfaces is more complex, little work has been recorded on randomly rough three-dimensional surfaces in which the roughness elements are irregular both in height and pitch.

On a rough surface, the dynamic behaviour of fluid is partly controlled by mass transfer, and this condition affects all transport processes. Since the research of Nikuradse [1], progressive work has been made towards basic understanding of the phenomenon on rough surfaces [2–19]. Most of the researchers have used the electrochemical method for studying this phenomenon [10,20–26]. This research has again utilized the electrochemical

* Tel.: +1 416 978 6901; fax: +1 416 978 8605.
*E-mail address:* s.lolja@utoronto.ca

0017-9310/$ - see front matter © 2005 Elsevier Ltd. All rights reserved.
doi:10.1016/j.ijheatmasstransfer.2004.12.030

**Nomenclature**

| | |
|---|---|
| $A$ | surface area of cathode [$m^{-2}$] |
| $a_i$ | coefficients in the correlating equations, $i = 1, 2, 3$ |
| $C$ | concentration of $Fe^{3+}$ ions; it is zero at the electrode wall in the diffusion-controlled conditions [mol $m^{-3}$] |
| $d$ | inner diameter of the pipe [m] |
| $D$ | diffusion coefficient [$m^2$ $s^{-1}$] |
| $e$ | height of roughness element [m] |
| $e^+$ | roughness Reynolds number |
| $f$ | dimensionless friction factor |
| $F$ | Faraday constant equals to 96,485 A s $mol^{-1}$ |
| $F(e^+)$ | friction similarity function |
| $v$ | velocity of flow [m $s^{-1}$] |
| $I$ | measured electric current [A] |
| $k$ | mass transfer coefficient [m $s^{-1}$] |
| $l$ | length of pipe [m] |
| $R$ | correlation coefficient |
| $Re$ | Reynolds number |
| $Sc$ | Schmidt number |
| $Sh$ | Sherwood number |
| $St$ | Stanton number |
| $z$ | number of electrons exchanged; to be one in this case |

*Greek symbols*

| | |
|---|---|
| $\Delta P$ | pressure drop between the entrance and exit points of the rough pipe [n $m^{-2}$] |
| $r$ | density of the solution [kg $m^{-3}$] |
| $\mu$ | dynamic viscosity [n s $m^{-2}$] |

*Subscripts*

| | |
|---|---|
| $b$ | in the bulk flow |
| lim | the limiting current obtained from the polarization curve and belonging to the sector which had no change in current when voltage was changed. |
| $w$ | at the electrode wall |

technique for studying the mass transfer at sandpaper-roughened surfaces, because such a technique causes no physical or chemical change on the rough surface.

The momentum transfer analysis has basically been done by expressing the friction factor from Eq. (1) as a function of Reynolds number. Then, two characteristic functions for rough surfaces were developed [1], as follows:

$$f = \frac{\Delta P}{\rho v^2}\frac{2d}{l} \tag{1}$$

The friction similarity function

$$F(e^+) = \left(\frac{8}{f}\right)^{0.5} + 2.5\ln\frac{2e}{d} + 3.75 \tag{2}$$

The roughness Reynolds number

$$e^+ = \frac{e}{d}Re\left(\frac{f}{8}\right)^{0.5} \tag{3}$$

The friction similarity function has been considered as a measure of frictional effect on the total pressure drop or the friction factor. The lower the curve of friction similarity function has been located on the graph, the greater has been the dependence of pressure drop on the roughness element height [9,18,19].

As to the mass transfer analysis, the local mass transfer rates can be accurately determined from the following system of cathodic reduction of the ferricyanide ion and anodic oxidation of ferrocyanide ion:

$$\text{Cathode} \quad Fe^{3+}\ (CN)_6^{3-} + e^- = Fe^{2+}\ (CN)_6^{4-}$$

$$\text{Anode} \quad Fe^{2+}\ (CN)_6^{4-} = Fe^{3+}\ (CN)_6^{3-} + e^-$$

This electrochemical method is implemented by operating under limiting current conditions (current is independent of cathode potential and ferricyanide ions react at once on the cathode surface), so that the cathode reaction becomes diffusion controlled. Under such conditions, the electrochemical reaction has the following three steps:

a. The diffusion of ions to the electrode, which is a process controlled by flow conditions, geometry, concentration of reacting species, and physical properties.

b. The reaction at the electrode surface, which is controlled by the temperature, geometry, surface conditions, and applied voltage.

c. The diffusion of reaction products from the electrode surface to the bulk flow. This step is strongly dependent on the concentration of products at the surface.

As the result of ionic reduction at the cathode and ionic oxidation at the anode, a current flows through the circuit by being proportional to the number of ions reacting at the electrodes per unit of time. At steady state conditions, ions converted at the electrode have to be supplied from the bulk of the liquid. The electrochemical reaction rate increases with the potential differ-

ence and, at a specific value of the applied voltage, the step of the diffusion of ions towards the electrodes becomes the rate-determining step in the entire electrochemical reaction. By using an extra large anode, the flux of reacting ions is mostly affected by the cathode geometry, and the entire electrochemical reaction depends on cathode diffusion. Hence, the average mass transfer flux of ferricyanide ions to cathode is:

$$N = k(C_b - C_w) = I_{lim}/zFA \ [\text{mol m}^{-2}\ \text{s}] \quad (4)$$

Since the electrochemical reaction of $Fe^{3+}$ ions at the electrode surface is immediate, it keeps to zero the concentration of $Fe^{3+}$ ions at the electrode surface. So, Eq. (4) is easily transformed to find the mass transfer coefficient, as follows:

$$k = I_{lim}/zFAC_b \ [\text{mol s}^{-1}] \quad (5)$$

Since steady-state conditions were kept in this research, the similitude transformation of general mass transfer equation gave the following mass transfer correlation:

$$Sh = a_1 Re^{a_2} Sc^{a_3} \quad (6)$$

Eq. (6) shows that the effect of Reynolds and Schmidt numbers onto Sherwood number is a combination of correlative coefficients $a_1$, $a_2$, and $a_3$. For analogy to the heat transfer similarity function [2], a mass transfer similarity function was developed and used in related research afterwards [4,8,20,22]. It resulted to be the ratio rough-to-smooth for Sherwood or Stanton number, as follows:

$$\frac{Sh_r}{Sh_s} = \frac{St_r}{St_s} = \frac{k_r}{k_s} = f(e^+, Sc) = a_1 (e^+)^{a_2} Sc^{a_3} \quad (7)$$

For analogy to Eq. (6) and referring to previous research, the dependency in Eq. (7) will be analysed in a power form. Since the function $f(e^+, Sc)$ depended on surface geometry, so did the Sherwood number ratio. Since, the Schmidt number physically relates the relative thickness of the hydrodynamic layer and the mass-transfer boundary layer, for any given Schmidt number and for a series of geometrically similar surfaces, a plot of the Sherwood number ratio versus roughness Reynolds number "$e^+$" should yield a single curve.

## 2. Experimental

Concentration of potassium ferri- and ferro-cyanides were 0.005 M and 0.03 M, respectively. The higher ferrocyanide concentration gave some protection against its anodic oxidation and, together with a larger anode than cathode area, caused the cathodic process to become rate determining. The solution temperature was 10 °C and 30 °C, and in such conditions the Schmidt number was 8520 and 2780, respectively. The necessary accurate values for the density and viscosity of the solution as well as the diffusivity of the ferricyanide ion have been taken from previous research [27].

The sandpaper-roughened surfaces were fabricated in the following way [16]: The mirror image of the sandpaper surface was prepared by pouring molten wood's metal (a composite of 12.5% Sn, 25% Pb, 50% Bi and 12.5% Cd) into the annulus of a glass container where the sandpaper was mounted on the inner surface of the container. The roughness pattern was imprinted onto the wood-metal body, which then was put into the nickel-electroplating bath (4 M solution of nickel sulfamate, pH = 5, air gurgling from the bottom to remove hydrogen bubbles at the cathode, voltage increased from 0.6 V and 0.125 A to 6.2 V and 0.8 A for 13 days). Boiling water was after used to melt the wood-metal and to obtain the nickel pipe with the required roughness pattern inside. The new-formed nickel cylinders were 3–4 mm thick and 340 mm long and were coded R100, R60 and R40 according to their respective standard names of the sandpaper source. The inner diameter of the pipes was 38 mm, and the average roughness heights were 0.11 mm (R100), 0.17 mm (R60), and 0.22 mm (R40). The Scattering Electron Microscopy showed typical irregularity for these rough surfaces.

The experimental set-up formed a recycling loop for pumping the solution out of a tank through a 3 m long PVC pipe to the nominated rough pipes (ordered as anode–cathode–anode), and then returned to the surge tank after passing the rotameter [15,25]. The long PVC pipe served the objective to reach and keep a well developed specific regime of flow before entering the nominated pipes. The change in fluid temperature was controlled by a cooling coil in the tank. Before experiments nitrogen was gurgled through the solution in the surge tank for 20 min and then at a lower rate. This was done to remove oxygen from the solution and create a blanket of nitrogen over the solution surface in the covered surge tank so oxygen could not re-dissolve to appreciable amounts. Experimenting was intensive because ferri/ferro-cyanide solution decays photo-chemically, though measures against light were taken.

The system used to obtain polarization curves (recorded and on screen) in this experiment consisted of the Radiometer Analytical S.A. PGZ301 Potentiostat Galvanostat Programmable Generator Electrochemical Impedance Meter connected by serial port to a computer with the Voltmaster-4 software installed. There were three electrode cables for experiments: working, reference and auxiliary. That device operated in Voltammeter $I = f(\text{V})$ mode where voltage varied from 0 to −2.0 V at a set sweep rate of 3 mV/s. The working electrode was connected to the cathode while both reference and auxiliary electrodes were linked to the connected anodes. The potentiostat enabled the use of a reference electrode to ensure the voltage applied was all at the cathode as conditions change. If using two anodes, one was linked

to the reference electrode and the other to the auxiliary electrode; however, this connecting system had no effect on the results, and thus it was not applied. When the electrical potential was applied between the two electrodes, the following three mass relocation conditions took place:

1. The ionic migration under the electric field. Intentionally, it was suppressed by adding highly conductive electrolyte (3 mol/l NaOH) which acts as inert at the applied voltage range of 0.0–2.0 V.
2. The mass transportation by convection due to bulk flow. Truly, it was eliminated at the wall, because the velocity perpendicular to the electrode was zero at the wall.
3. The mass transfer by diffusion due to the concentration gradient. Since this was the remaining route for mass relocation, the transportation close to the wall was essentially by both molecular and Eddy diffusions, and their contributions were included in the mass transfer coefficient.

## 3. Results and discussions

### 3.1. Momentum transfer analysis

The experimental measurements and calculation results are put in Fig. 1, which shows that the values of Reynolds number fall between 6500 and 140,000. For smooth pipes, the Blazius model describes rightly the momentum transfer for Reynolds number up to 100,000. Since the higher the Reynolds number, the smaller the thickness of the viscous sub-layer, beyond $Re = 100{,}000$ the experimental friction factor deviates upward from Blazius model aiming at fully developed region, because the viscous sub-layer almost does not exist now and the pipe is not anymore hydraulically smooth. Now, the bulk flow is in real contact with the given surface which is not ideally smooth. That is, a drag force even exists between the bulk flow and the not-ideally smooth surface, and it is cause of the deviation from the Blazius model for $Re > 100{,}000$.

Fig. 1 show that the coarser the surface, the smaller the Reynolds number where the friction factor starts to move away upward from the Blazius model heading for fully developed region; that is, the higher the friction factor generated or the higher the pressure drop recorded. In the fully developed region or the so-called the auto-modelled region, the friction factor will be independent from Reynolds number: the curve will be parallel to the Reynolds number (abscise) axis. Referring to previous research, Fig. 1 is converted into a graph of rough-to-smooth friction factor ratio versus Reynolds number, nothing special is observed: the experimental sequences have a tendency to increase (from one to about a value of two) with the increase of Reynolds number by staying over the Blazius line which is parallel to abscise axis in this new graph [1,4,14,15,18,19].

Though the above results and curves are in accordance with the results achieved in previous research [1,4,14,15,18,19], a difference exists in the gained values (lower values in friction factor) due to the peculiarity of the surfaces and the method used in this research for producing the rough surfaces. In particular, a difference exists with Nikuradse's data who produced rough surfaces by gluing uniformly sized sand grain particles; his rough surfaces had uniformity of roughness elements in terms of particle size, height, pitch, particle slopes, and particle edge sharpness. This difference is also seen on the Fig. 2 which bonds the friction similarity function and roughness Reynolds number. The obtained experi-

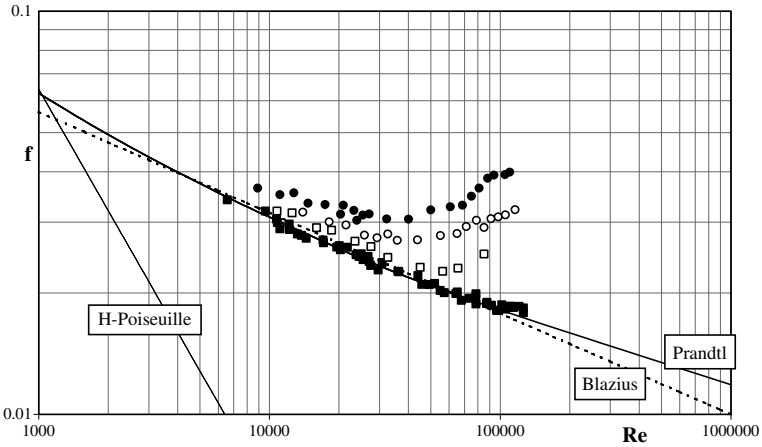


Fig. 1. Friction factor for the three rough surfaces and smooth surface, where: (□) for R100, (○) for R60, (●) for R40, (■) for smooth pipe.

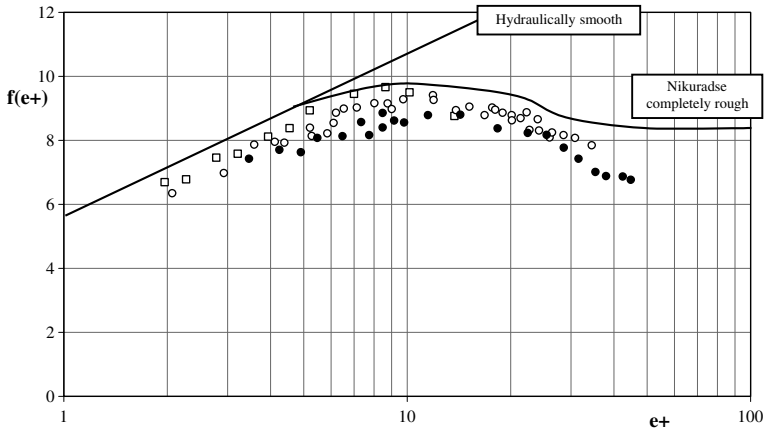


Fig. 2. Friction similarity function versus roughness Reynolds number, where: (□) for R100, (○) for R60, (●) for R40.

mental points do not overlap the Nikuradse's curve and that of hydraulically smooth regime, but stay below and even follow their curve shapes. That is, some geometric similarity exists between the present surfaces and the Nikuradse's surfaces. Though the points pertaining to all surfaces can be grouped as a single set of data in Fig. 2, undoubtedly the coarser the surface, the more distance from the Nikuradse curve exists. Both shapes of experimental curves and Nikuradse curve (passing through a maximum) indicate that the transition towards the fully developed regime of flow on rough surfaces is not straightforward.

On the other hand, the rough surfaces produced from images of sandpaper in this research have less uniformity of the roughness elements in terms of particle size, height, pitch, particle slopes, and in particular, the particle edges are smoother. Having non-uniform grain sizes and random particle positioning, the fluid flow paths become longer and more chaotic, and so more fluid energy or velocity is lost due to the shear stress and the frictional drag force is higher. Also, Scattering Electron Microscopy micrographs of the surfaces under study exhibit three-dimensional irregularity. However, the three rough surfaces constitute a roughness series, for they originated from a sandpaper series.

The dependence between the rough-to-smooth friction factor ratio and roughness Reynolds number is put in Fig. 3. The experimental points look much better fused to each other as a single set, and also well positioned against the Nikuradse curve which moves tangentially along them. With a correlation coefficient of 0.958, the set of all points is described by the equation $f_r/f_s = 1.0082*\exp[0.0194*(e^+)]$. This correlation gives a reasonable basis for concluding that the series of rough surfaces display friction similarity. These results make the "$e/d$" factor more important than the roughness height "$e$" in characterising the set of surfaces. Fig. 3 shows that for $e^+ < 3$, all roughness systems start to become hydraulically smooth as they approach to $f_r/f_s = 1$. Obviously for $e^+ < 3$, the viscous sub-layer thickness at the wall begin to suppress the roughness distinction, thus resulting to the hydraulically smooth state represented by the fluid smoothness. It is noted that the value $e^+ = 1$ belongs to the middle of hydraulic transition region from laminar to turbulent region.

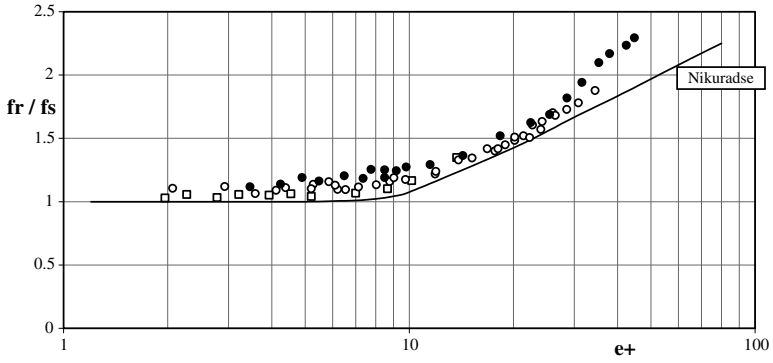


Fig. 3. Friction factor ratio versus roughness Reynolds number, where: (□) for R100, (○) for R60, (●) for R40.

### 3.2. Mass transfer analysis

The results of experimental measurements and calculations are put in Fig. 4, whereas correlation results are presented in Table 1. For comparative reasons, the correlative equations in the form of Eq. (6) belonging to the smooth-surfaced pipe were taken from previous research [15], and they were represented by the plain lines on Fig. 4. Such pipes were made of Nickel from the same technique as used in this research for making rough surface pipes and had the same dimensions; also, these mass transfer results for the smooth surface had strongly been reconfirmed by other researchers [6,7,22,25].

As seen on Fig. 4, in the range of Reynolds number between 200 and 60,000, either the higher the Reynolds number or the coarser the surface or higher the value of Schmidt number, the higher the mass transfer is. This is supported by the fact that the power coefficients "$a_2$" and "$a_3$" in Table 1 have positive sign. Points are more scattered in the laminar region than in the turbulent region and with a trend to converge to higher values of Reynolds number. For all cases in Fig. 4, the curve slope in laminar region is smaller than that in turbulent region. Table 1 reveals very good correlation coefficients, which also are strong in specific cases: at a given flow regime, rough surface, and Schmidt number. This is a proof that the found correlations based on the Eq. (6) describe very well the experimental profiles of mass transfer in the range of Reynolds number studied in this research.

From Table 1 and for a given rough surface, the increase of Reynolds number is associated with the decrease of coefficient $a_1$ (smaller contribution from undistinguished parameters), the increase of coefficient $a_2$ (higher contribution from turbulence), and the decrease of coefficient $a_3$ (less contribution from the characteristics of the fluid). In laminar region and for each of rough pipes R60 and R40, the contribution of Schmidt number is twice bigger than that of Reynolds number ($a_3/a_2 \approx 2$). This reconfirms the idea that for small fluid velocity (the fluid viscous sub-layer just at the surface is thicker), the characteristic properties of the fluid, such as viscosity, density, and diffusivity (which constitutes the Schmidt number) determines the overall mass transfer process. In laminar region, a rougher surface brings about the decrease of coefficient "$a_1$", but increasing coefficients "$a_2$" and "$a_3$".

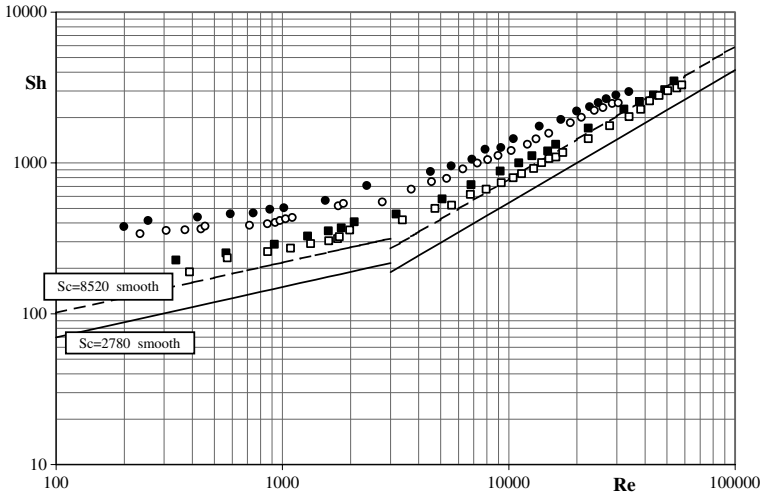


Fig. 4. Sherwood number versus Reynolds number, where: (●) is for pipe R40, 10 °C, $Sc$ = 8520; (○) is for pipe R60, 10 °C, $Sc$ = 8520 (■) is for pipe R40, 30 °C, $Sc$ = 2780; (□) is for pipe R60, 30 °C, $Sc$ = 2780.

Table 1
Correlation results for Eq. (6)

| Pipe-flow | $Sc$ | $Re$ | $a_1$ | $a_2$ | $a_3$ | $R$ |
|---|---|---|---|---|---|---|
| R40-laminar | 2780, 8520 | 200–2080 | 2.215 | 0.214 | 0.439 | 0.980 |
| R40-turbulent | 2780, 8520 | 4510–53,750 | 0.206 | 0.706 | 0.252 | 0.995 |
| R60-laminar | 2780, 8520 | 230–1980 | 3.826 | 0.190 | 0.375 | 0.972 |
| R60-turbulent | 2780, 8520 | 4560–58,100 | 0.068 | 0.777 | 0.284 | 0.995 |
| Ref. [4] | 390, 4590 | 3000–120,000 | 0.153 | 0.88 | 0.32 | |
| Ref. [10] | 550, 4720 | 6000–60,000 | 0.134 | 0.68 | 0.39 | |

For all rough pipes in Table 1, the contribution of Schmidt number to mass transfer in turbulent flow is smaller than that of Reynolds number; even, the coarser the surface, the bigger the times the Reynolds number surpassed the Schmidt number (higher the ratio $a_2/a_3$). Obviously again, more turbulence causes the viscous sub-layer just at the wall to be much thinner, and thus reaching higher rate of mass transfer between the bulk flow and the wall. In addition, a rough surface in turbulent region is associated with the increase of coefficient "$a_1$", and the decrease of coefficients "$a_2$" and "$a_3$". Within the Reynolds number range of 200–60,000 and for both rough surfaces, the sum of coefficients "$a_2$" and "$a_3$" is $0.61 \pm 0.05$ for the laminar region, and $1.01 \pm 0.05$ for the turbulent region; such a sum is 1.14–1.2 for the smooth surface in the turbulent region. Also from Tables 1 and 2, these coefficients bear similarity to the respective values found for other types of rough surfaces [4,10,13,15,17,20,22].

In order to assess the mass transfer enhancement on rough surfaces against the smooth surface, the ratio rough-to-smooth mass transfer coefficient "$Sh_r/Sh_s$" can be either plotted versus the Reynolds number or the roughness Reynolds number. Since the last relates linearly to the Reynolds number, Eq. (3), both curves would have (as proved) the same shape. Therefore, pursuing the modelling function given by Eq. (7), the mass transfer enhancement will be analysed versus the roughness Reynolds number only. As seen in Fig. 5, the data points of the same roughness appear as a single set, in particular, at high roughness Reynolds number. This is a confirmation of what is previously said for the mass transfer similarity function. Also, the rougher the surface, the higher the mass transfer similarity function represented by the ratio "$Sh_r/Sh_s$". All curves have a drop for $1 < e^+ < 10$ from a value of about 2.3 to 1.3, and the finer the surface, the sooner the drop. Obviously, the increase of Reynolds number or the roughness Reynolds number is coupled with the increase of turbulence and the decrease of viscous sub-layer thickness. Consequently, the contribution of the induced turbulence by the surface roughness becomes less important. For $e^+ > 10$ ($Re > 30{,}000$), all curves become almost parallel to abscise axis, and even tend to congregate. That is, for

Table 2
Correlation results for Eq. (7) in turbulent flow

| Pipe | $a_1$ | $a_2$ | $Sc$ | $a_3$ | $R$ |
|---|---|---|---|---|---|
| R40 | 2.032 | −0.124 | 2780 | | 0.973 |
| R40 | 2.466 | −0.239 | 8520 | | 0.988 |
| R40 | 2.138 | −0.182 | 2780, 8520 | 0.00654 | 0.941 |
| R60 | 1.640 | −0.095 | 2780 | | 0.835 |
| R60 | 2.036 | −0.234 | 8520 | | 0.989 |
| R60 | 1.439 | −0.149 | 2780, 8520 | 0.02769 | 0.886 |
| Ref. [4], $e^+ > 25$ | 1.94 | −0.10 | 390, 4590 | 0.09 | 0.967 |
| Ref. [10], $e^+ > 10$ | 1.79 | −0.17 | 550, 4720 | 0.12 | |

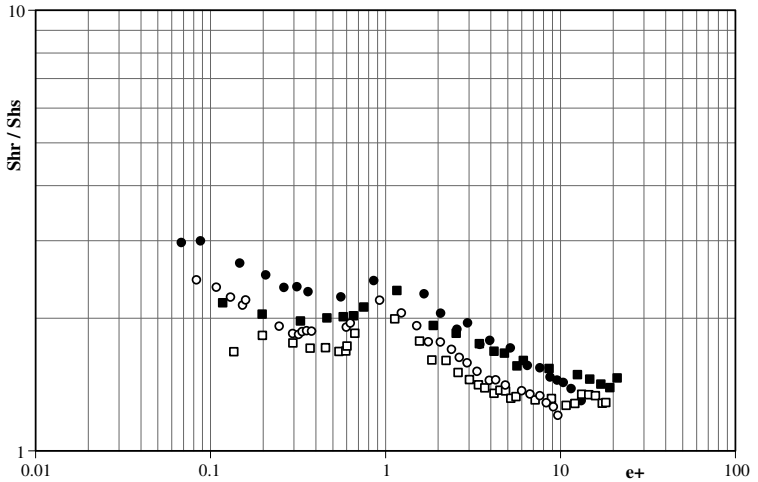


Fig. 5. Mass transfer similarity function versus roughness Reynolds number, where: (●) is for R40, 10 °C, $Sc = 8520$; (○) is for R60, 10 °C, $Sc = 8520$; (■) is for R40, 30 °C, $Sc = 2780$; (□) is for R60, 30 °C, $Sc = 2780$.

$e^+ > 10$ ($Re > 30{,}000$), the roughness distinction on mass transfer similarity function fades away, and the mass transfer enhancement does not change anymore but keeps an average value of about 1.34. This reconfirms what is concluded in the preceding graphs and in the end of the Introduction section. However, more data in the region $e^+ > 20$ ($Re > 60{,}000$) would complete the shapes of curves on Fig. 5.

An explanation ought to be added in respect with Fig. 5. No frictional data were obtained for the laminar region, which were required to calculate the roughness Reynolds number. However, by looking at curves on Figs. 2 and 3, and by finding with calculation that the roughness Reynolds number had an exponential dependence against the sole Reynolds number (with correlation coefficient $R > 0.99$), then it was concluded to extend such an exponential correlation in the laminar region too. That assumption proved to be correct, because the shapes of mass transfer similarity function versus Reynolds number were (as found) the same as those versus roughness Reynolds number in Fig. 5.

The data points in Fig. 5 are more scattered in the laminar region. For $e^+ < 0.8$ ($Re < 2000$), the sequence of the experimental points differs from those reported previously [4,15]; it disagrees least for the surface R60 at $Sc = 2780$ and most for the surface R40 at $Sc = 8520$. Hence, such data may be received with some uncertainty, because the relative gain in mass transfer $Sh_r/Sh_s$ was generally expected going to one or somehow parallel to $Sh_r/Sh_s = 1$ when roughness Reynolds number goes to unity [4,15]. In any case, a drop tendency exists in the laminar region from a value of not more than three to about two or less. The surfaces at low Reynolds number are hydraulically smooth, that is, roughness height is smaller than the viscous sub-layer height. It looks as taking a small rise before entering the transition region, and followed afterwards by a steeper descent in the turbulent region. Since the low rate of molecular diffusion very near the wall is the major resistance to mass transfer process, any induced turbulence caused by surface roughness prompts a greater increase in mass transfer rates, in particular in the lower diffusivity systems (higher Schmidt number). Consequently, the data points in Fig. 5 are more scattered in the laminar region; in a way, this enlightens the importance of surface roughness and flow disturbances caused by surface defects or surface geometric profile. Even the tiniest amount of turbulence have an effect on mass transfer rate when the Schmidt number is high enough (the diffusion coefficient is small).

For the turbulent region in Figs. 5 and 6, the tendency of the experimental points is similar to but shifted left and with relative gain in mass transfer being smaller due to the fact that the roughness heights are smaller than those reported previously [4,13,15]. In turbulent flow, results in Table 2 demonstrate very good correlation coefficients for Eq. (7), in particular when Schmidt number is constant for a given rough surface; the exception is the case of pipe R60 at $Sc = 2780$, which reveals a correlation coefficient of 0.84. For pipe R40 in Table 2, the power exponents for the roughness Reynolds number and Schmidt number are $-0.18$ and 0.0065, respectively; for pipe R60, they are $-0.15$ and 0.027, respectively. Obviously, such results indicate the Reynolds number to be a more affecting factor than Schmidt number.

Whenever the enhancement of mass transfer is desirable, it ought to be reached at minimal operational cost. For fluid transportation, the operational cost is directly connected to the energy spent to move the fluid. There-

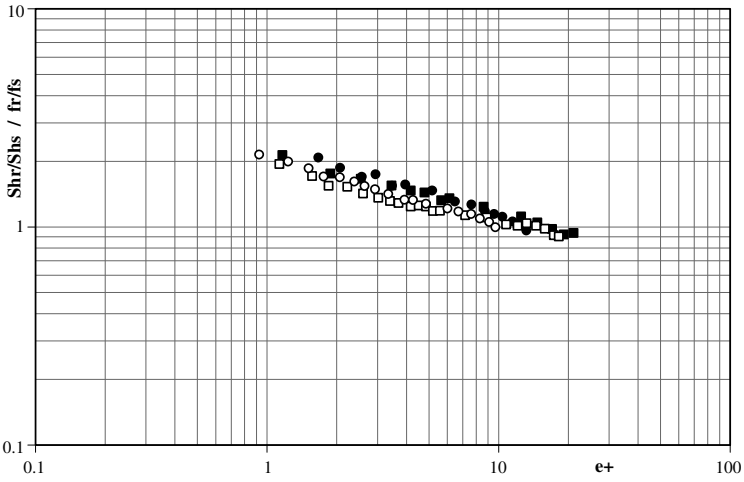


Fig. 6. Mass transfer efficiency index versus roughness Reynolds number, where: (●) is for R40, 10 °C, $Sc = 8520$; (○) is for R60, 10 °C, $Sc = 8520$; (■) is for R40, 30 °C, $Sc = 2780$; (□) is for R60, 30 °C, $Sc = 2780$.

Table 3
Correlation results for Eq. (8) in turbulent flow

| Pipe | $Sc$ | $a_1$ | $a_2$ | $R$ |
|---|---|---|---|---|
| R40 | 2780 | 2.179 | −0.277 | 0.995 |
| R40 | 8520 | 2.439 | −0.338 | 0.991 |
| R60 | 2780 | 1.820 | −0.237 | 0.984 |
| R60 | 8520 | 2.092 | −0.312 | 0.997 |
| All data | 2780, 8520 | 2.044 | −0.272 | 0.956 |

fore, the ratio of mass transfer enhancement coefficient ($Sh_r/Sh_s$) to friction enhancement coefficient ($f_r/f_s$) is defined as the mass transfer efficiency index [4,15,25], which is analysed in a power form, as follows:

$$\frac{Sh_r/Sh_s}{f_r/f_s} = a_1(e^+)^{a_2} \tag{8}$$

The mass transfer efficiency index is given in Fig. 6 as a function of roughness Reynolds number, but only for the turbulent region wherein experimental frictional data were available. The data points are merged to each other with a small distinction between the pipe R60 (smoother) and the pipe R40 (rougher). Obviously, the smoother pipe points (R60) stand below the rougher pipe points (R40) in Fig. 6. Either separately or as an entire set, the data points in Fig. 6 are well correlated by Eq. (8). The results are put in Table 3, which shows that the Schmidt number determines the power exponent "$a_2$" as of being about "−1/4" for $Sc = 2780$, and "−1/3" for $Sc = 8520$.

For the type of rough surfaces used in this research, Fig. 6 demonstrates that the maximum efficiency (equal to two) is for $e^+ = 1$ ($Re = 3000$). Beyond such values, the mass transfer efficiency index decreases but keeping values higher than one. Further than $e^+ = 10$ ($Re = 30{,}000$), the mass transfer efficiency index keeps decreasing but beginning to bear values less than one. That is, the gain in mass transfer enhancement is positive versus the friction development only in the Reynolds number range of 3000–30000 ($e^+ = 1$–10). Reconfirming what is said before, the reason for decreasing mass transfer efficiency index with the increase of Reynolds number is that the flowing system is going towards a fully turbulent regime with enough kinetic energy not to be disturbed by the type of roughness used in this research. This means that the roughness effect onto flowing parameters, such as turbulence degree or the viscous sub-layer thickness, keep decreasing.

## 4. Conclusions

It is clear that the coarser the surface, the smaller the Reynolds number where the friction factor starts to turn aside upwards from the course of Blazius model. The fact that the recorded friction factor curves stay lower than that of Nikuradse indicates that the fabricated rough surfaces of this research had roughness elements with sharper edges than those of Nikuradse. The shape of friction similarity function curves points out that the transition towards fully developed regime of flow on the considered rough surfaces is not straightforward and smooth. It is adequate to use friction factor behaviour alone for characterising a rough surface. Plots of mass transfer similarity function indicates that the general form of the similarity function depends on size, shape and spacing of the roughness elements, flow geometry, and solution conditions. Each specific rough surface displays its own characteristic profiles, and irregular surfaces gives irregular response.

It is shown that mass transfer is increased with the Reynolds number, the surface roughness and Schmidt number. With the increase of Reynolds number, the mass transfer enhancement is less affected by undistinguished parameters, more affected by flow turbulence, and less affected by fluid characteristics. For $Re > 30{,}000$ or $e^+ > 10$, the mass transfer enhancement expressed by the mass transfer similarity function converges to an average value of 1.34. The correlative results for the mass transfer efficiency index versus Reynolds number or roughness Reynolds number may be used as an excellent predictive criterion for similar cases. The mass transfer improvement versus friction development is acceptable only for $Re = 3000$–$30{,}000$ or $e^+ = 1$–10.

A more powerful pump is required to complete the surface behaviour data in very high Reynolds number. Further experiments can also be conducted to cover wider ranges of $Fe^{3+}$ concentration, cell voltage, Reynolds number, and solution temperature. Correlations developed in the laminar and turbulent regions for such distributions may give more insight into convective or diffusive mass transfer mechanisms. In the future, more surfaces of variable mass transfer areas can be created employing the technique used in this research. An analytical solution for given boundary conditions will lead to theoretical results to be compared with experimental results, and will give a fundamental understanding as to how different surfaces affect the mass transfer rate. Data availability for frictional, mass transfer, and heat transfer enhancements will provide knowledge on heat-mass-transfer analogies. With such essential knowledge for predicting the equipment performance, heat and mass exchangers with rough surface in the fluid-solid interface can be designed.

## Acknowledgement

The author is grateful to the support received from Prof. Olev Trass and the Department of Chemical Engineering at the University of Toronto.

## References


[1] T. Nikuradse, Laws of flow in rough pipes, V.D.I. Forschungsheft 361, Series B, 1933. (NACA TM 1291, 1950).

[2] F. Dipprey, R.H. Sabersky, Heat and momentum transfer in smooth and rough tubes at various Prandtl numbers, International Journal of Heat Mass Transfer 6 (5) (1963) 329–353.

[3] B.K. Mahato, L.W. Shemilt, Effect of surface roughness on mass transfer, Chemical Engineering Science 23 (2) (1968) 183–185.

[4] D.W. Dawson, O. Trass, Mass transfer at rough surfaces: square duct flow, transverse V-shaped grooves, International Journal of Heat Mass Transfer 15 (7) (1972) 1317–1336.

[5] A.M. Yaglom, B.A. Kader, Heat and mass transfer between a rough wall and turbulent fluid flow at high Reynolds and Peclet number, Journal of Fluid Mechanics 62 (3) (1974) 601–723.

[6] S. Treiber, Surface characterization and mass transfer at randomly rough, electroplated and sintered surfaces in square duct flow, M.Sc. Theses, Department of Chemical Engineering, University of Toronto, 1974.

[7] A. Martineau, Surface characterization and mass transfer at randomly rough electroplated surfaces in square duct flow, M.Sc. Theses, Department of Chemical Engineering, University of Toronto, 1976.

[8] B.A. Kader, A.M. Yaglom, Turbulent heat and mass transfer from a wall with parallel roughness ridges, International Journal of Heat and Mass Transfer 20 (4) (1977) 345–357.

[9] D.C. Leslie, The form of the extended Reynolds analogy for rough surfaces, Letters in Heat and Mass Transfer 5 (2) (1978) 99–109.

[10] F.P. Berger, K.-F. Hau, F.-L. Hau, Local mass/heat transfer distribution on surfaces roughened with small square ribs, International Journal of Heat and Mass Transfer 22 (12) (1979) 1645–1656.

[11] S.C. Tantirige, O. Trass, Mass transfer at geometrically dissimilar rough surfaces, Canadian Journal of Chemical Engineering 62 (3) (1984) 490–496.

[12] M. Grimanis, B. Abedian, Turbulent mass transfer in rough tubes at high Schmidt numbers, Physicochemical Hydrodynamics 6 (6) (1985) 775–787.

[13] J. Grifoll, X. Farriol, F. Giralt, Eddy diffusivity equation for high Schmidt number mass transfer at regular rough surfaces, International Communications in Heat and Mass Transfer 14 (6) (1987) 721–729.

[14] S.C. Tantirige, A.P. Iribarne, M. Ojha, O. Trass, The turbulent boundary layer over single V-shaped grooves, International Journal of Heat and Mass Transfer 37 (15) (1994) 2261–2271.

[15] W.C. Zhao, O. Trass, Electrochemical mass transfer measurements in rough surface pipe flow: geometrically similar V-shaped grooves, International Journal of Heat and Mass Transfer 40 (12) (1997) 2785–2797.

[16] N. Gehani, C. Ng, High Schmidt number mass transfer enhancement at irregular rough surfaces in pipe flow, B.Eng.'s Thesis, University of Toronto, 1999.

[17] N. Mahinpey, M. Ojha, K.W. Johnston, O. Trass, Electrochemical mass transfer measurements in Y-Bifurcation model, Canadian Journal of Chemical Engineering 78 (5) (2000) 902–906.

[18] P.R. Chandra, C.R. Alexandera, J.C. Hanb, Heat transfer and friction behaviours in rectangular channels with varying number of ribbed walls, International Journal of Heat and Mass Transfer 46 (3) (2003) 481–495.

[19] K. Ceylan, G. Kelbaliyev, The roughness effects on friction and heat transfer in the fully developed turbulent flow in pipes, Applied Thermal Engineering 23 (5) (2003) 557–570.

[20] T.K. Ross, A.A. Wragg, Electrochemical mass transfer studies in annuli, Electrochimica Acta 10 (11) (1965) 1093–1106.

[21] J.R. Selman, C.W. Tobias, Unsteady-state effects in limiting current measurements, Journal of Electroanalytical Chemistry 65 (1) (1975) 67–85.

[22] F.P. Berger, K.-F.F.-L. Hau, Mass transfer in turbulent pipe flow measured by the electrochemical method, International Journal of Heat and Mass Transfer 20 (11) (1977) 1185–1194.

[23] P.P. Grassmann, Applications of the electrolytic method. Advantages and disadvantages, mass transfer between a falling film and the wall, International Journal of Heat and Mass Transfer 22 (6) (1979) 795–798.

[24] J.R. Selman, C.W. Tobias, Mass transfer measurements by the limiting current technique, Advanced Electro-Chemical Engineering 10 (2) (1988) 211–318.

[25] N. Mahinpey, M. Ojha, O. Trass, Transient mass and heat transfer in a smooth pipe, International Journal of Heat and Mass Transfer 44 (20) (2001) 3919–3930.

[26] J. Gosticka, M. Pritzker, A. Lohib, H.D. Doanb, Mass transfer variation within a packed bed and its relation to liquid distribution, Chemical Engineering Journal 100 (1–3) (2004) 33–41.

[27] J.R. Bourne, P. dell'Ava, O. Dossenbach, Th. Post, Densities, viscosities, and diffusivities in aqueous NaOH potassium-ferri-and-ferro-cyanide solution, Journal of Chemical Engineering Data 30 (1) (1985) 160–163.